Watenphul, A., Wunder, B., Wirth, R., Heinrich, W. (2010): Ammonium-bearing clinopyroxene: A potential nitrogen reservoir in the Earth's mantle. - Chemical Geology, 270, 1-4, 240-248

DOI: 10.1016/j.chemgeo.2009.12.003

Ammonium-bearing clinopyroxene: A potential nitrogen reservoir in the Earth's mantle

Anke Watenphul*, Bernd Wunder, Richard Wirth, and Wilhelm Heinrich

Deutsches GeoForschungsZentrum (GFZ), Telegrafenberg, 14473 Potsdam, Germany, Section 3.3 * E-mail: watenphul@gfz-potsdam.de

Abstract

In the pseudobinary system $CaMgSi_2O_6 - (NH_4)M^{3+}Si_2O_6$, with M = Cr or Al, and NH_4OH in excess, multi-anvil experiments at 9.5 to 12.8 GPa, 725 to 750 °C produced NH_4-bearing diopside. Incorporation mainly follows the coupled substitution $(Ca^{2+})_{M2} + (Mg^{2+})_{M1} \Leftrightarrow (NH_4^+)_{M2} + (M^{3+})_{M1}$. Ammonium was identified and quantified by IR spectroscopy. In Cr-bearing diopside we found maximum concentrations in the range of 500 to 1000 ppm of NH_4.

The storage capacity of mantle clinopyroxenes for ammonium turns them to potential candidates for the nitrogen reservoir in the Earth's upper mantle, and this mechanism also contributes to its water budget. While nitrogen is transported into the mantle via cold slabs through NH_4 inherited from sedimentary material, and stored in K-bearing minerals and successor high-pressure phases, nitrogen output from the mantle is through degassing of N_2. A probable mechanism for that is that nitrogen is kept as NH_4 in clinopyroxene in the Earth's mid and lower mantle, whereas in the upper part, it is lost due to oxidation to molecular nitrogen. It is most likely that clinopyroxene plays a major role in the long-time, large-scale nitrogen cycle between surface and deep mantle of the Earth.

Keywords: Ammonium; Clinopyroxene; Nitrogen cycle; High pressure; IR spectroscopy; Earth's mantle

Introduction

Studies on the nitrogen cycle in deep Earth have shown that the input of nitrogen from the Earth's surface to depth occurs through subduction of ammonium-bearing sediments and altered oceanic crust. In most environments nitrogen is soon released to the surface via arc volcanism (e.g., Sano et al., 2001; Fischer et al., 2002) or lost during increasing metamorphic grade (Bebout and Fogel, 1992; Bebout et al., 1999; Sadofsky and Bebout, 2000; Mingram and Bräuer, 2001; Pöter et al., 2004; Plessen et al., *in revision*). By contrast, at cold slab conditions nitrogen remains in the rocks at least down to 90 km and very probably beyond the depth locus of island arc magmatism (Busigny et al., 2003a). This is because the ammonium cation, NH_4^+, inherited from organic material, has a similar ionic radius as Rb^+ and can replace K^+ in the respective K-bearing phases (e.g., Williams et al., 1992).

Experimental work has shown that the NH_4-analogues of the ultrahigh-pressure K-bearing phases phengite, K-cymrite, K-Si-wadeite, and K-hollandite are successively stable with increasing pressure – at least to 12 GPa in the case of NH_4-hollandite – provided that redox conditions are reducing enough to stabilize NH_3/NH_4^+ relative to molecular nitrogen, N_2 (Watenphul et al., 2009). This supports the idea that substantial amounts of nitrogen are recycled into the deep mantle. Busigny et al. (2003a) presented a mass balance indicating that currently about 3 to $5 \cdot 10^{10}$ mol nitrogen are annually transported to greater depths via cold slabs. At the other end of the deep nitrogen cycle, molecular nitrogen, N_2, is discharging from the Earth's mantle for a long time in hydrothermal and volcanic activities (e.g., Javoy et al., 1986; Marty, 1995). It has been suggested that the main nitrogen release would take place at mid-ocean ridges (Sano et al., 2001). Another approach ascribes the overall nitrogen output mainly to volcanic arcs (Hilton et al., 2002). As the case may be, an important issue remains unclear so far, namely if and how nitrogen could be stored to significant amounts in upper mantle assemblages, i.e., in peridotitic rocks.

Regarding the major phases in peridotites, clinopyroxene represents the most probable candidate for incorporation of NH_4. There is experimental evidence that clinopyroxene can uptake K_2O by several weight% at pressures between 7 and 14 GPa through the coupled substitution $(Ca^{2+})_{M2} + (Mg^{2+})_{M1} \Leftrightarrow (K^+)_{M2} + (M^{3+})_{M1}$ (Harlow 1997; Safonov et al., 2003; Harlow and Davies, 2004), where M^{3+} stands for Al or Cr. Omphacitic clinopyroxenes from ultrahigh-pressure rocks have been reported to uptake potassium within the same concentration range (Perchuk et al., 2002; Bindi et al., 2003). Following the rationale of NH_4 substituting K in mineral structures, it is possible that NH_4 may be incorporated into ultrahigh-pressure clinopyroxene by the same mechanism.

In this contribution we test whether high-pressure clinopyroxene is a potential host for nitrogen in the Earth's mantle by performing experiments in a multi-anvil apparatus. We will show that Cr-bearing clinopyroxene can incorporate NH_4 concentrations by up to 1000 ppm at relevant P–T conditions, and argue that its storage capacity for NH_4 might represent the nitrogen reservoir in the upper mantle. We finally speculate on the role that clinopyroxene might play during the long-time, large-scale nitrogen cycle between Earth's surface and depth.

Table 1. Starting materials, experimental conditions, run durations, and run products.

Run no.	$X_B^{Bulk\ a}$	P (GPa)	T (°C)	t (h)	Run products (wt%)
AW24-08	0.1	11.5	750	8	NH_4-Di (66), Stv (24), Grt (10)
AW01-09	0.1	12.8	725	5	NH_4-Di (81), Gy (10), Stv(6), En (3)
AW18-08	0.5	9.5	750	10	NH_4-Di (∼70), Gy (∼20), Grt (∼2), unkn. phase 1 (∼8)
AW23-08	0.5	11.5	750	6	NH_4-Di (53), Stv (31), Gy (13), Grt (3), Cr-Top (< 1)
AW25-08[b]	0.2	11.5	750	8	NH_4-Di (∼45), Stv (∼28), Grt (∼17), Ky (∼5), unkn. phase 2 (∼5)

Abbreviations: NH_4-Di=NH_4-bearing diopside, Stv=stishovite, Grt=garnet, Gy=guyanaite, Ky=kyanite, En=enstatite, Cr-Top=$Cr_2SiO_4(OH)_2$, unkn. phase 1=unknown phase with d = 4.87 Å, 2.67 Å, unkn.phase 2=unknown phase with d = 2.32 Å, 2.73 Å.
[a] X_B^{bulk} = proportion of hypothetical $NH_4M^{3+}Si_2O_6$ mixture in the starting bulk composition.
[b] run with Al_2O_3 instead of Cr_2O_3.

Experimental and Analytical methods

Synthesis

Inherent difficulties arise when NH_4-bearing minerals are synthesized at high-pressure. Using heated gels as starting materials is almost impossible, because ammonium is rapidly evaporated during heating. Thus, we used stoichiometric oxide mixtures of SiO_2, $Ca(OH)_2$, MgO, Cr_2O_3, and Al_2O_3 as starting solids. MgO, Cr_2O_3, and Al_2O_3 were pre-heated at 700 °C for several hours. Ammonium was introduced as 25% NH_4OH solution in excess. Starting bulk compositions consisted of different proportions of two mixtures, a stoichiometric diopside mixture A [$CaMgSi_2O_6$] and a hypothetic mixture B [$(NH_4)M^{3+}Si_2O_6$], with M^{3+} being either Cr or Al. Bulk compositions of the starting mixtures are listed in Table 1.

Stabilization of NH_4-bearing phases requires some NH_3/NH_4^+-gas pressure. Hence, excess NH_4OH solution is needed to produce a sufficiently high partial pressure of ammonia and to keep the hydrogen fugacity high, i.e., the redox conditions reducing, at least as long as the H–N–O fluid provides enough hydrogen at any given pressure and temperature. We used gold capsules surrounded by hexagonal boron nitride (h-BN) to minimize hydrogen loss during the course of the run. A detailed description of the experimental setup is given in Watenphul et al. (2009). In addition, about 4 mg of TiH_2 were placed outside of the Au-capsules as supplementary source for hydrogen, following the method of Pal'yanov et al. (2002).

Experiments were performed in a multi-anvil apparatus at 360°-rotation of the Walker-type module with a rate of 5°/s to prevent separation of fluid and solid components. We used 14/8 pressure assemblies (octahedron edge length/anvil truncation edge length). Temperature was measured using a W5%Re–W26%Re (Type C) thermocouple with a precision of about ± 10 °C. Pressure calibration was performed by press-load experiments based on several room and high-temperature phase transitions. The estimated pressure uncertainty is about ± 0.2 GPa.

By using this setup, the experimental temperatures are limited to a sample temperature of about 800 °C in the applied pressure range. This is because the actual temperatures of the h-BN spacers in direct contact with the furnace are much higher. If higher sample temperatures were applied, the h-BN spacer would undergo a phase transition to the cubic structure, which induces a large volume change and, consequently, a failure of the experiment.

After the experiments the capsules were carefully separated from the assembly material and cleaned with ethanol in an ultrasonic bath for 10 min. Analysis of any ammonium, possibly from outside contamination of the crystals due to quench fluids, is avoided by washing the run products with warm bi-distilled water and subsequent drying at 100 °C for several days.

Powder X-ray diffraction (XRD)

About 1 mg of the run products was ground for several minutes in an agate mortar, diluted with Elmar's white glue and spread evenly on a "zero scattering" foil. Preferential orientation of the crystals was minimized by constantly stirring the sample during the drying process. The sample was covered with an empty foil and mounted onto a transmission sample holder. Powder XRD patterns were recorded in transmission with a fully automated STOE STADI P diffractometer using CuKα_1-radiation at 40 kV and 40 mA, a take-off angle of 6°, a primary monochromator, and a 7° wide position-sensitive detector (PSD). The intensity was recorded between 5° and 125° 2θ with a detector step size of 0.1° and a resolution of 0.02°. The counting time was chosen such that the maximum intensity resulted in about 3500 to 4000 counts. The collected pattern was processed using the GSAS software package for Rietveld refinement (Larson and von Dreele, 2004) for phase identification, determination of phase proportions, and refinement of unit cell parameters. Crystal structures were taken from the Inorganic Crystal Structure Database (ICSD, FIZ Karlsruhe, http://icsdweb.FIZ-Karlsruhe.de).

The statistical parameters χ^2 and Durbin-Watson (DW) of the Rietveld refinements of the runs AW23-08, AW24-08, and AW01-09 are within the ranges of $1 < \chi^2 < 1.2$ and $1.3 < \mathrm{DW} < 1.5$. The run products AW18-08 (Cr-bearing) and AW25-08 (Al-bearing) included an unidentified phase. Phase proportions of the unknown phases in these two runs were estimated by comparison of their reflection intensities with that of all other known phases. Statistical parameters were within the ranges of $1 < \chi^2 < 1.5$ and $1.0 < \mathrm{DW} < 1.3$. The obtained unit cell parameters of all phases from these runs are reliable despite of the uncertainty in the phase proportions.

Infrared spectroscopy (IR)

Infrared spectroscopic measurements were carried out on KBr pellets. 2 mg of the run products were ground in an agate mortar and mixed homogeneously with 450 mg pre-dried KBr. This mixture was pressed under vacuum to 13 mm diameter pellets and dried for several days at 170 °C.

Measurements at room temperature and temperature-dependent measurements at -180 °C, 20 °C, and 200 °C were carried out with a Bruker IFS 66v FTIR spectrometer equipped with a Graseby Specac P/N 21525 variable temperature cell, respectively. We

used a globar as light source, a KBr beam splitter and a DTGS detector. The sample chamber of the interferometer was evacuated down to 200 Pa, therefore, interference of atmospheric H_2O and CO_2 was negligible.

Spectra were taken in the region from 4000 to 400 cm^{-1} with a resolution of 2 cm^{-1} and averaged over 256 scans. The interferograms were phase-corrected after the procedure of Mertz (1965) and Griffiths and de Haseth (1986). The Blackman-Harris 3-term mode was chosen as apodization function. All spectra were fitted using the program PeakFit by Jandel Scientific. Background correction was uniformly carried out in the region from 1550 to 1350 cm^{-1}, because the NH_4-ν_4 absorption band in cpx is located around 1414 cm^{-1} (see below). Absorption bands were fitted with a mixed Gaussian and Lorentzian distribution function.

NH_4 concentrations c_{NH_4} were calculated according to the Lambert–Beer-law:

$$c_{NH_4} = M_{NH_4} \times A^{\mu}_{NH_4} / (t \times \rho_{cpx} \times \epsilon^{\mu}_{N-H}) \quad (1)$$

where M_{NH_4} is the molecular weight of the absorbing species, t the sample thickness, ρ_{cpx} the density of the absorbing sample, ϵ^{μ}_{N-H} the molecular absorptivity of the corresponding N–H vibration at a certain wavenumber μ, and $A^{\mu}_{NH_4}$ the related absorbance in the IR spectrum corrected to 100 wt% diopside in the sample. Because molar absorption coefficients for NH_4 in pyroxenes are currently not available, their NH_4 concentrations are estimated based on a mean molecular absorptivity, which was determined for micas (Busigny et al., 2003b, Busigny et al. 2004). The plausibility of this procedure is explained below.

The thickness of the absorbing pyroxene is determined by the difference in thickness between a KBr pellet, which contains sample powder, and a pure KBr pellet. Such differential measurements were identically performed for all samples, and resulted in an averaged thickness of 20 μm. Calculations applied a density value for cpx of 3.315 g/cm^3, which is an averaged value, calculated from our Rietveld refinements.

A similar procedure was used for estimation of traces of OH concentrations of additional phases produced in the runs.

Electron microprobe analysis (EMP)

Polished grain mounts of each sample were analyzed using a JEOL JXA-8500F field emission electron microanalyzer in the wavelength-dispersive mode (WDS). As standards diopside (Ca, Mg, Si), Cr_2O_3 (Cr), and orthoclase (Al) were used. Nitrogen could not be measured because concentrations were below the EMP detection limit. The operation conditions were 15 kV, 10 nA, with a beam diameter of about 50 nm. On-peak counting times were 20 s for all elements. Background on both sides of the peak was measured for 10 s.

Some NH_4-bearing diopsides contained solid inclusions of a Cr-rich phase (Fig. 1a). The size of the inclusions was too small for EMP analysis. Special care was taken in choosing analysis spots to avoid contamination by the inclusions.

Transmission electron microscopy (TEM)

Thin foils of diopsides from runs AW23-08 and AW24-08 were prepared by the focused ion beam (FIB) technique (Wirth, 2009) for TEM analyses. The foils, about 8 μm × 10 μm

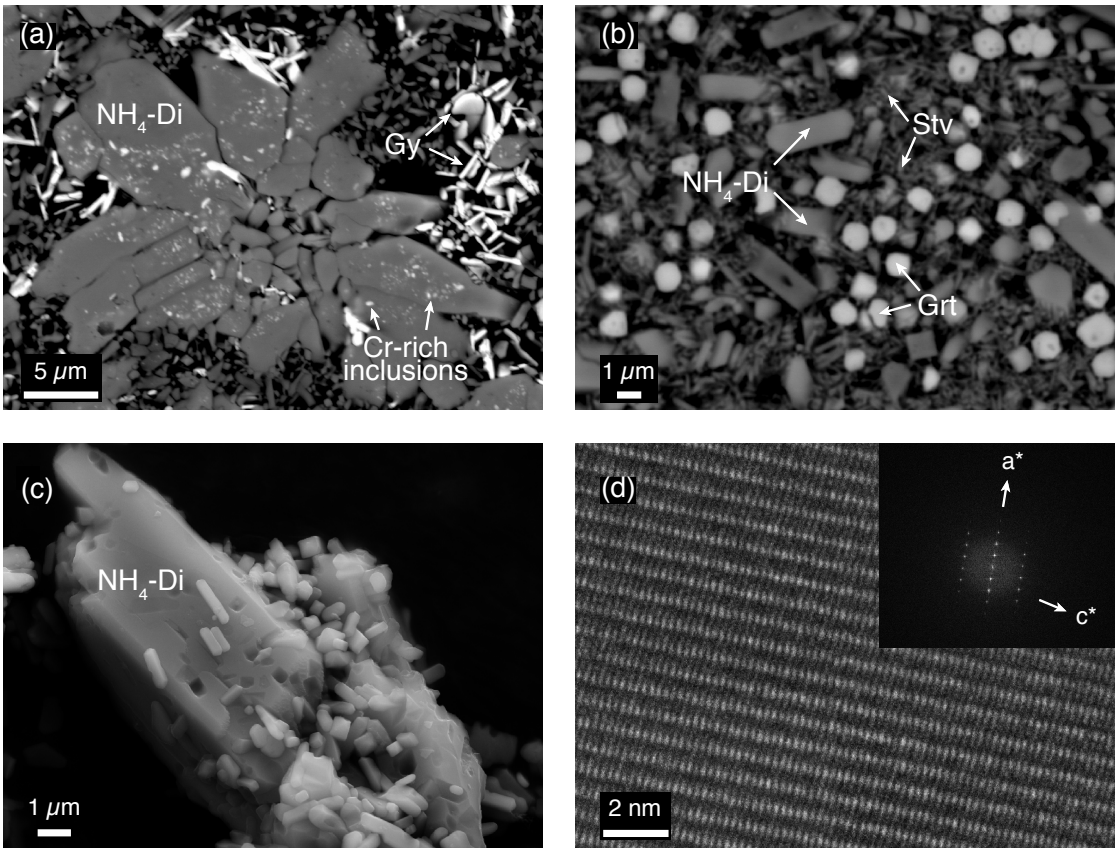

Figure 1: Microprobe images of the run products: (a) run AW23-08 produced diopside (large crystals) with Cr-rich inclusion, probably guyanaite. (b) run AW24-08 contains smaller inclusion-free diopside. (c) Scanning electron micrograph of run AW23-08 showing a large (10 μm) long diopside. (d) HRTEM image displaying lattice fringes of a diopside from run AW23-08, along with the corresponding SAED pattern.

in size with thickness between 100 to 200 nm, were placed on a TEM copper grid. ATEM analyses were carried out using a FEI Tecnai G^2 transmission electron microscope equipped with a field emission cathode. Operation conditions were 200 kV, condenser aperture 3, spot size 9, and a tilt angle of 20°. Beam damage of the samples was minimized by applying frames of about 150 nm × 100 nm for the energy dispersive X-ray (EDX) analyses. Counting time was 120 s.

Inclusions of the Cr-rich phase appeared also in the bright-field image overview of the diopside foil from run AW23-08 (Fig. 2a). Their sizes ranged from micro- to nanometers. Hence, frames set for EDX analysis were chosen from high-angle annular dark field (HAADF) images (Fig. 4.2b), so that inclusions were avoided. EDX spectra were analyzed for Mg, Si, Ca, and Cr. The data were corrected for background, absorption, and internal K_{AB}-factors using the TIA software package. The relative total errors were Mg, Ca (4 %), Si (3 %), and Cr (min. 50 %).

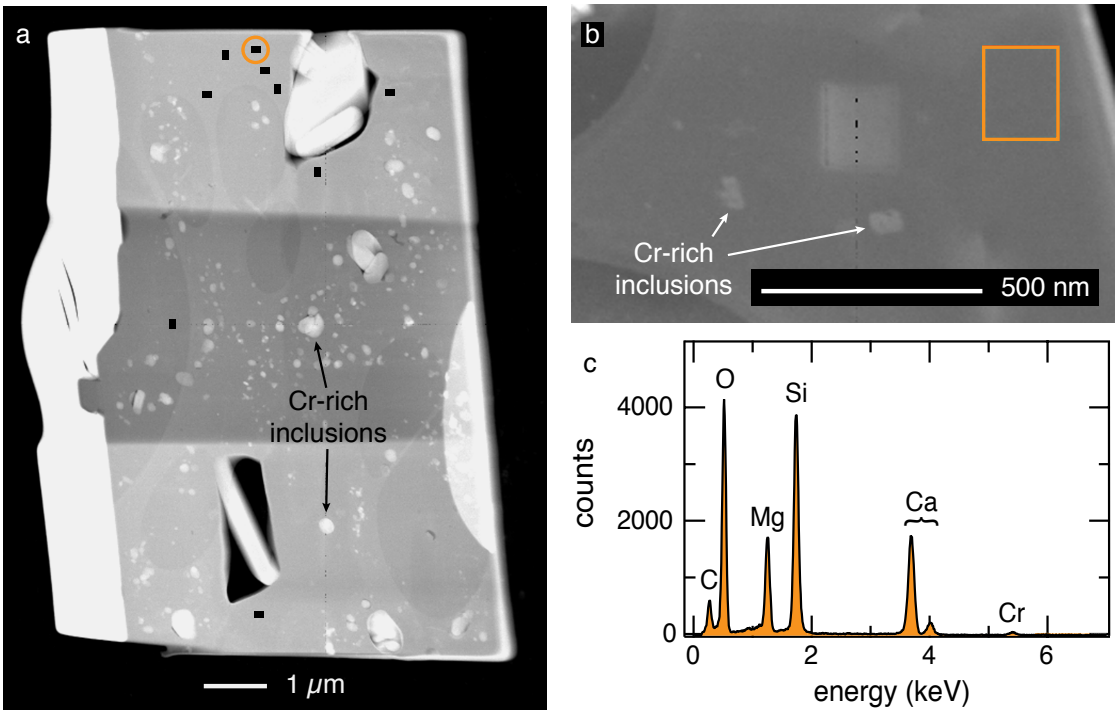

Figure 2: (a) Bright-field image of the FIB foil cut from a diopside of run AW23-08. Center of the foil (dark gray) is thinner than the parts above and below. Black rectangles mark positions of the EDX measurements. (b) Enlarged portion of the FIB foil. Frame indicates the encircled measuring spot in (a). (c) EDX spectrum corresponding to the frame marked in (b).

Attempts to quantify nitrogen with electron energy loss spectroscopy (EELS) were not successful. This might be due to rapid amorphization of the sample foil during spectra acquisition, concentrations not far from the detection limit, and the position of the N K-edge at the broad shoulder of the Ca K-edge. Nitrogen is a trace element here, and its K-edge is very weak compared to that of Ca. Its intensity is therefore difficult to estimate after background correction.

Thin foils were also used for high-resolution imaging of the lattice fringes of the diopsides. For that, a foil thickness of about 100 nm or less is required. Fourier transformation of high-resolution images resulted in diffraction patterns that contained the identical information as the selected area electron diffraction (SAED) patterns on the same sample foil (Fig. 1d).

Scanning electron microscopy (SEM)

A Gemini ultra high-resolution FE-SEM from Zeiss was used to characterize the reaction products (Fig. 1c). Individual phases with measurable sizes were identified by EDX analysis of the respective elements. The operation conditions were 20 kV, a point size beam diameter and on-spot counting times of 60 s. The resulting EDX spectra were comparable with those

determined by ATEM.

Results

The proportions of the $CaMgSi_2O_6 - (NH_4)M^{3+}Si_2O_6$ mixtures in the starting bulk compositions, experimental conditions, run durations, and relative amounts of solid run products are summarized in Table 1. NH_4-bearing diopside was produced in all experiments as the main solid phase with varying proportions from 45 to 81 wt% of the run products. Additional phases, identified by Rietveld refinement, are present in various amounts.

In Cr-bearing runs NH_4-bearing diopside is formed together with stishovite, garnet, which is very rich in uvarovite [$Ca_3Cr_2(SiO_4)_3$] component, and/or guyanaite [CrOOH], whereas the latter is only present if the starting bulk composition is very rich in chromium. Run AW01-09 produced minor amounts of enstatite, run AW23-08 yielded traces of the Cr end member of topaz-OH [$Cr_2SiO_4(OH)_2$]. Cr-topaz-OH was identified in the IR spectrum due to almost identical OH bands as observed for topaz-OH. The position of one of these bands is slightly shifted, and both display the identical splitting at -180 °C as observed for the Al-analogue (Watenphul and Wunder, 2009). Run AW18-08 additionally produced an unidentified phase in minor amounts (∼8 wt%).

The Al-bearing run AW25-08 produced NH_4-bearing diopside along with stishovite, garnet, rich in grossular [$Ca_3Al_2(SiO_4)_3$] component, kyanite, and small amounts of an unidentified phase (∼5 wt%).

Fig. 1a–c show EMP and SEM backscattered micrographs of representative run products. NH_4-bearing diopside forms idiomorphic crystals with typical monoclinic crystal shapes (Fig. 1c), and grain sizes varying between 1 to 25 μm. Larger crystals from runs with high Cr content in the starting mixture (runs AW18-08, AW23-08, AW01-09) contained micro- to nanometer-sized inclusions of a Cr-rich phase, which is very probable guyanaite (Fig. 1a). Small NH_4-bearing diopsides (run AW24-08) are free of solid inclusions (Fig. 1b). Accompanying phases were too small in size (1 μm and below) to be analyzed for chemical composition.

Unit cell dimensions of NH_4-bearing diopside from all samples are given in Table 2 along with that of a pure reference diopside, which was hydrothermally synthesized from a mixture of $CaCO_3$, MgO, and SiO_2 plus H_2O in excess at 0.3 GPa, 750 °C, and a run duration of 9 days. The a and b lattice parameters of the NH_4-bearing diopsides are slightly smaller compared to the reference diopside.

Lattice fringe images of NH_4-bearing diopsides from run AW23-08 (Fig. 1d) and AW24-08 showed that there are no chain multiplicity faults present. Also, the crystals are free of other defects.

Reliable EMP analyses were difficult to obtain due to problems with solid inclusions in NH_4-bearing diopside (runs AW18-08, AW23-08, and AW01-09), and the small crystal size of NH_4-bearing diopsides (runs AW24-08, AW25-08). The determined Cr and Al contents presented in Table 3 are associated with a relatively high degree of uncertainty and represent average values of about 15 analyses for each sample.

A typical EDX spectrum taken from the diopside foil of sample AW23-08 is shown in Fig. 2c. The orange square in Fig. 2b displays the analysis frame, which is free of solid

Table 2. Lattice parameters of NH_4-bearing diopsides calculated from Rietveld refinements.

Run no.	a (Å)	b (Å)	c (Å)	β (°)	V (Å^3)
Diopside[a]	9.7500(7)	8.9279(5)	5.2510(3)	105.834(6)	439.74(6)
AW24-08	9.741(1)	8.919(1)	5.2529(4)	105.861(6)	439.02(9)
AW01-09	9.739(1)	8.9178(7)	5.2530(4)	105.874(6)	438.88(7)
AW18-08	9.738(2)	8.915(2)	5.252(1)	105.89(1)	438.5(1)
AW23-08	9.732(2)	8.912(1)	5.2547(9)	105.89(1)	438.3(1)
AW25-08	9.742(2)	8.918(1)	5.2532 (7)	105.85(1)	439.1(1)

[a] single-phase diopside ($CaMgSi_2O_6$) hydrothermally synthesized at 0.3 GPa, 750 °C, run duration: 9 d.
2σ uncertainties given in parentheses apply to the last digit.

inclusions. The electron beam may cause minor damage to the foil, visible by a slightly brighter rectangle in the center of the HAADF image (Fig. 2b), which resulted from an earlier frame analysis. The carbon peak, visible in the spectrum, is due to the carbon coating of the foil. The observed relative intensities of Ca, Mg, Si, and O are typical for diopside. There is a significant Cr peak in all spectra, which corresponds to the concentration of 1.30(46) wt% Cr_2O_3 in AW24-08, and 0.83(40) wt% Cr_2O_3 in AW23-08 (Table 3). This is roughly in line with EMP analyses. Cr_2O_3 contents are averaged values over 10 analyses for each sample.

Room temperature IR spectra of the run products of all runs are presented in Fig. 3a. Spectra display a distinctive absorption band in the spectral region of around 1414 cm^{-1}, which is assigned to the NH_4 bending vibration ν_4 (see Watenphul et al., 2009). That this band represents indeed the NH_4-ν_4 vibration is confirmed by the shift of the band position with temperature (Fig. 3b). The NH_4-ν_4 vibration of runs AW23-08, AW01-09, and AW24-08, respectively, gains intensity upon cooling and shifts from 1431 cm^{-1} at -180 °C to 1397 cm^{-1} at 200 °C, typical for vibrations in which hydrogen is involved. In the vicinity of the NH_4-ν_4 band further weak bands appear at somewhat higher wavenumbers (Fig. 3a), which are attributed to overtones of lattice vibrations. Unlike the NH_4-ν_4 vibration, the lattice vibrations display only very minor shifts of less than 8 cm^{-1} along the temperature

Table 3. NH_4 and Cr concentrations determined from IR, EMP, and ATEM, respectively.

Run no.	NH_4 (wt ppm)	Al_2O_3 (wt%)	Cr_2O_3 (wt%)	Cr_2O_3 (wt%)	NH_4 (apfu)	Al (apfu)	Cr (apfu)	Cr (apfu)
Method	IR	EMP	EMP	ATEM	IR	EMP	EMP	ATEM
AW24-08	177(80)	-	0.90(33)	1.30(46)	0.002(1)	-	0.013(3)	0.019(7)
AW01-09	428(200)	-	1.02(50)	-	0.005(2)	-	0.015(7)	-
AW18-08	481(200)	-	1.33(50)	-	0.006(2)	-	0.019(7)	-
AW23-08	1014(450)	-	1.68(36)	0.83(40)	0.012(5)	-	0.024(10)	0.012(6)
AW25-08	92(70)	1.5(7)	-	-	0.001(1)	0.017(8)	-	-

1σ-uncertainites for NH_4 and 2σ for Al/Cr concentration apply to the last digit(s).

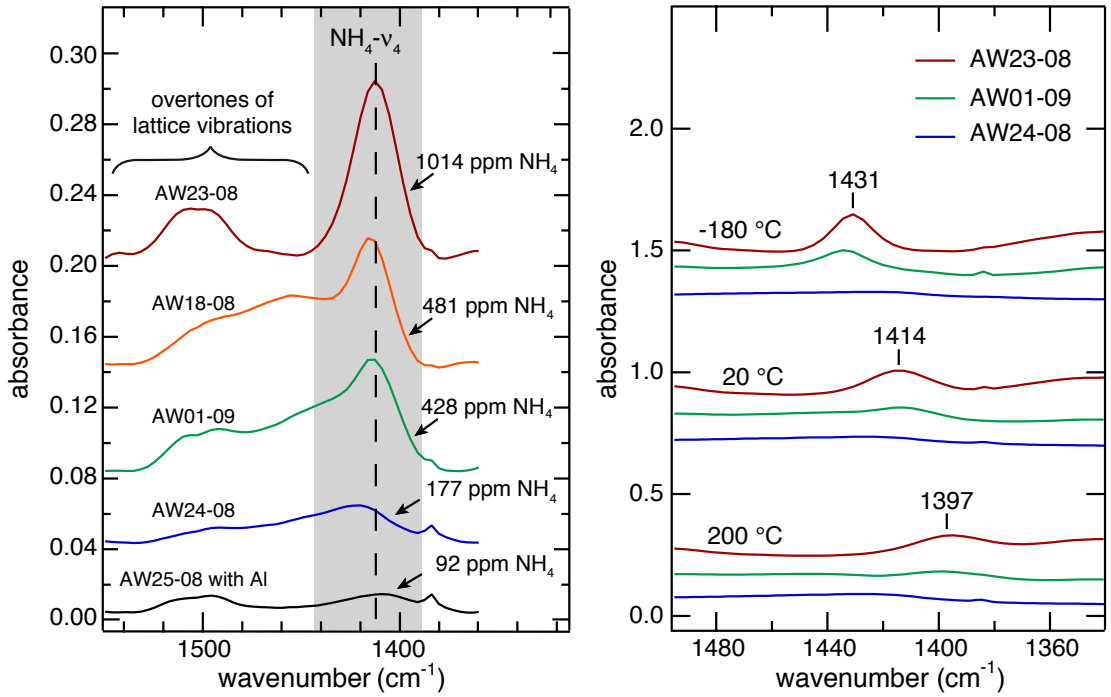

Figure 3: (a) Mid-infrared spectra in the spectral range from 1550 to 1360 cm^{-1} of run products from AW23-08 (1014 ppm NH_4), AW18-08 (481 ppm NH_4), AW01-09 (428 ppm NH_4), AW24-08 (177 ppm NH_4) and AW25-08 (92 ppm NH_4). Gray shaded area emphasizes the NH_4-ν_4 bending mode; vertical dashed line marks the position. (b) Mid-infrared spectra in the spectral range from 1490 to 1347 cm^{-1} of the run AW23-08, AW01-09 and AW24-08 as a function of temperature. The position (in cm^{-1}) of the NH_4-ν_4 bending mode is marked. All spectra are offset for clarity.

range of -180 °C to 200 °C, and can therefore be clearly distinguished from the NH_4-ν_4 band. Because the NH_4 concentrations in diopside are low, relatively large amounts of sample material are required to obtain an NH_4 signal. Hence, the intensities of the lattice vibrations (normal modes not shown in Fig. 3a) are high and overtones around 1500 cm^{-1} are visible.

Diopside is the predominant solid phase in the run products and the sole one that could host small but significant amounts of NH_4. Crystal chemical constraints for clinopyroxene require charge balance for the trivalent cation, Cr^{3+}, sitting at the M1 position, and it is most plausible that this is done via incorporation of the monovalent NH_4^+ into M2, rather than by Cr^{3+} incorporation into the tetrahedral site (see below). Furthermore, it is highly unlikely that the additional phases stishovite and guyanaite could significantly incorporate NH_4^+, which is also true for the traces of kyanite in the Al-bearing sample. Wang and Takahashi (1999) showed that below 22.5 GPa garnets virtually do not uptake K_2O. Because NH_4 is only incorporated in K-bearing phases, all garnets of this study are considered ammonium-free. Minute amounts of enstatite occur in one, and minor amounts of an unknown phase

in only two samples, and these are therefore considered as not being responsible for the observed IR signal in all samples.

Thus, incorporation of NH_4^+ at the diopside M2 site accounts for the NH_4-ν_4 absorbance. If so, measured intensities allow for calculation of NH_4 concentrations. By using eq. (1), concentrations between 177 and 1014 ppm NH_4 result for the four Cr-bearing samples, and about 92 ppm for the Al-bearing sample (Table 3, Fig. 3a).

XRD patterns in combination with IR spectra provide information on additional phases in the run products. Guyanaite-containing samples AW18-08, AW23-08, and AW01-09 display small very broad and diffuse absorbances between 3670 and 3000 cm^{-1}, which are interpreted as the OH stretching bands of guyanaite. The IR spectrum of AW23-08 additionally shows two small OH stretching bands at 3600 and 3530 cm^{-1}. Upon cooling at -180 °C, the two bands split into four, revealing identical behavior as observed for topaz-OH (Watenphul and Wunder, 2009). Thus, Cr-topaz-OH must account for these bands. The IR spectrum of the Al-bearing sample AW25-08 displays a weak OH stretching band at 3563 cm^{-1}, together with broad shoulders at the low-energy wing. This band is interpreted as belonging to the OH incorporation into garnet (e.g., Beran and Libowitzky, 2006). The lattice parameter a of this garnet was determined to 11.755(1) Å, corresponding to $Grs_{81}Py_{19}$ solid solutions if a simple grossular-pyrope binary is assumed. Using an averaged molar absorption coefficient ϵ of 12500 l mol^{-1} cm^{-2} for OH in grossular-rich garnet (Maldener et al., 2003), measured intensities are converted to OH concentrations applying the procedure described above. It results that about 1000 ppm H_2O are incorporated. Samples containing uvarovite-rich garnet show no distinctive bands in the OH stretching region. Similarly, there is no hint for OH incorporation into NH_4-bearing diopsides.

Discussion

NH_4 concentrations and the incorporation mechanism into diopside

IR spectroscopy is the only direct method for the identification and quantification of the incorporated amount of NH_4 into diopside. The free ammonium ion, NH_4^+, has T_d symmetry resulting in four internal vibration modes, NH_4-ν_1 to NH_4-ν_4. From these, only the symmetric stretching vibration NH_4-ν_3 between 3350 and 3200 cm^{-1}, and the antisymmetric bending vibration NH_4-ν_4 around 1430 cm^{-1} are IR-active (positions from high-pressure NH_4-phases from Watenphul et al., 2009). The reported IR spectra of NH_4-bearing minerals and synthetic solid phases always display NH_4-ν_4 as the most intense vibration of the NH_4-tetrahedron. Therefore, this is probably the only vibration that is visible in IR spectra at low NH_4 concentrations. With regard to all solid phases investigated so far, the NH_4-ν_4 positions vary over about 20 cm^{-1}, due to the different crystal structures and local environments involved. In diopside, the NH_4-ν_4 band is located around 1414 cm^{-1}, at somewhat lower wavenumbers compared to other NH_4-bearing high-pressure phases such as NH_4-hollandite, NH_4-Si-wadeite, NH_4-cymrite, and NH_4-phengite(Watenphul et al., 2009) but still higher than for the free NH_4^+ cation (at 1397 cm^{-1}; Herzberg, 1966).

The unambiguous identification of the NH_4-ν_4 vibration is confirmed by heating and cooling the NH_4-bearing diopside containing samples while recording IR spectra. The bandshift of the NH_4-ν_4 vibration averages about 30 cm^{-1} between -180 and 200 °C, which is about

the same as the shift of the ND_4-ν_4* vibration in ND_4-tobelite [$(ND_4)Al_3Si_3O_{10}(OH)_2$] between -253 and 7 °C (Mookherjee et al., 2002). Compared to the relatively large bandshift of NH_4-ν_4, the lattice vibrations shift only about 5 to 8 cm^{-1} over the relevant temperature range. This is mainly because the X–O bonds (X = Si, Ca, Mg, Cr, Al) of the lattice forming atoms are much stronger than the N–H bonds of the NH_4 tetrahedron.

The NH_4 concentrations are calculated with a molar absorption coefficient of $\epsilon^{\mu}_{N-H} = 451.5 \pm 32$ l mol^{-1} cm^{-1}, which is an average value of the molar absorption coefficients of the NH_4-ν_4 bands at 1430 cm^{-1} in muscovite (Busigny et al., 2003b) and biotite (Busigny et al., 2004). The uncertainty corresponds to the minima and maxima for each value. The resulting concentrations vary between 92 and 1014 ppm NH_4 (Table 3). It is clear that the absorption coefficients of NH_4 in diopside and mica must be different, due to significant differences in crystal structure and density. Thus, the presented concentrations are approximate values, which can be potentially corrected once better absorption coefficients are available. A procedure to estimate a correction to the molar absorption coefficient for NH_4 in diopside would make use of the bandshift of the NH_4 stretching vibrations between muscovite/biotite and NH_4-bearing diopside. This shift would provide a measure for the difference in strength of the N–H bonds in both minerals, which directly correlates with the change of the absorption coefficient. Unfortunately, the NH_4 stretching frequencies are invisible in our spectra because NH_4 concentrations are too low. However, even if the absolute NH_4 concentrations presented in Table 2 and Figure 3 were slightly different from the "true" values, a correction would shift all values towards the same direction. Accordingly, the following considerations about the incorporation mechanism of NH_4 into diopside would still hold true.

In K-bearing clinopyroxene, potassium is incorporated into M2 via the coupled substitution $(Ca^{2+})_{M2} + (Mg^{2+})_{M1} \Leftrightarrow (K^{+})_{M2} + (M^{3+})_{M1}$. It is reasonable to assume that a similar mechanism holds also for the NH_4 incorporation. If so, the molar concentrations of NH_4 and Cr or Al, respectively, should be equal. Assuming the ideal diopside end member, the concentrations of the NH_4 and M^{3+} per formula unit (Table 3) are calculated under the assumptions that (1) every mol NH_4 is balanced by the equal proportion of M^{3+} and vice versa, and that (2) NH_4 substitutes for Ca in M2 and M^{3+} for Mg in M1. Fig. 4 shows that a coupled exchange of $(NH_4^{+})_{M2} + (M^{3+})_{M1} \Leftrightarrow (Ca^{2+})_{M2} + (Mg^{2+})_{M1}$, within error limits, is only valid for NH_4-bearing diopside produced in run AW23-08, and for Cr concentrations determined by ATEM. NH_4-bearing diopsides from other runs display somewhat lower NH_4 concentrations at similar contents of M^{3+}. Despite of the fact that the concentrations of Cr and Al in the starting compositions were very high, we measured a maximum solubility of (Cr,Al) in NH_4-bearing diopside of about 0.025 atoms pfu at the given P-T range. Saturation in the Cr, Al-bearing systems is always ensured, because the additional phases Cr-rich garnet, guyanaite or kyanite were present in the runs (Table 1).

The excess of M^{3+} in NH_4-bearing diopside relative to NH_4 might have several reasons: (1) The actual NH_4 concentrations have relatively large uncertainties, as our applied molar absorption coefficient for NH_4 is only a rough estimation. However, if we would evenly correct our measured intensities to higher NH_4 concentrations this would, for AW23-08, result in an NH_4 excess relative to the trivalent cation, which is highly unlikely. (2) Additional substitution mechanisms are active. Possible candidates for that are (i) the incorporation of an Ca-Eskolaite component [$Ca_{0.5}\square_{0.5}M^{3+}Si_2O_6$], or (ii) incorporation of M^{3+} into the

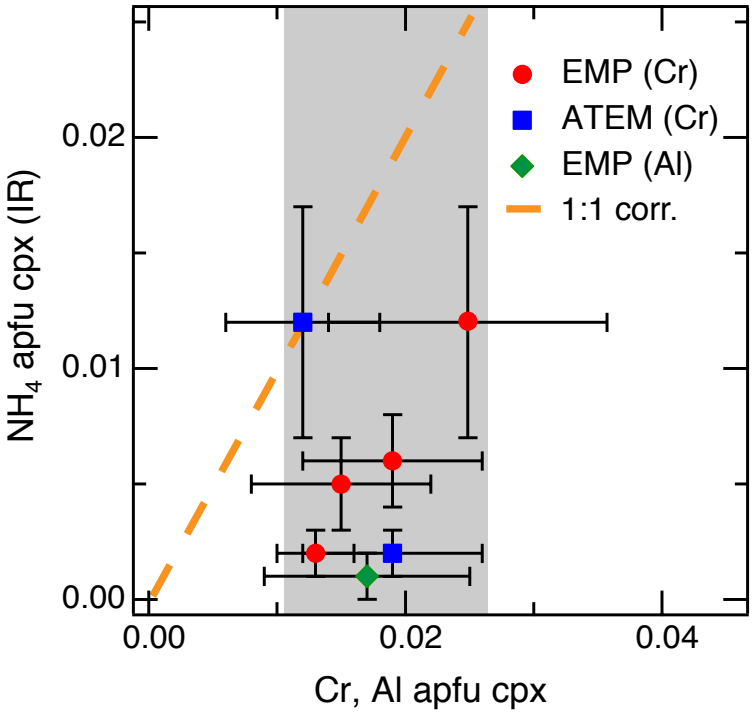

Figure 4: Plot of the calculated NH_4 concentrations (pfu) from IR measurements versus measured (Cr,Al) concentrations (pfu) from EMP and ATEM analyses. Gray shaded area emphasizes the measured M^{3+} concentrations within the errors. Dashed line gives the 1:1 correlation, which indicates the charge-balanced coupled substitution $NH_4^+ + M^{3+} \Leftrightarrow Ca^{2+} + Mg^{2+}$.

tetrahedron via Ca-Tschermak's substitution $[(Mg^{2+})_{M1} + (Si^{4+})_T \Leftrightarrow (M^{3+})_{M1} + (M^{3+})_T]$. Aside from that incorporation of small amounts of Mg on the Ca position is also possible, representing a small clinoenstatite component [$Mg_2Si_2O_6$]. This substitution would not explain the M^{3+} excess in most NH_4-bearing diopsides. (3) The varying NH_4 concentrations may also be due to changing redox conditions during the course of the experiments. Reducing conditions are a prerequisite for the formation of NH_3/NH_4^+ in the mineral–fluid system and for preventing oxidation to N_2. In all experiments a large excess of NH_4OH was used that kept the redox conditions sufficiently reducing. This enabled the formation of NH_4-bearing diopside in the presence of NH_3-bearing fluid. However, with our experimental setup loss of hydrogen into the pressure medium during the course of the experiment could not be completely avoided. This would imply that molecular nitrogen is produced and that the NH_3/NH_4^+ partial pressures were continuously reduced. Hence, it is possible that the NH_4-bearing diopsides in our quench products were partially decomposed, and it is not unlikely that some of the Cr-rich nanoinclusions, probably representing guyanaite, might stem from this partial decomposition process. (4) Differences in pressure might explain the different NH_4 concentrations measured in NH_4-bearing diopsides from AW23-08 (at 11.5 GPa; 1014 ppm NH_4) and AW18-08 (at 9.5 GPa; 481 ppm NH_4), for which all other variables

were identical. It would appear that within our experimental range temperature plays a minor role on the incorporation mechanism.

An important result is that the occurrence of significant amounts of OH defects in the crystal structure of the NH_4-bearing diopsides is excluded. No bands were visible in the IR spectra that could be related to OH incorporation.

The unit cell dimensions of the NH_4-bearing diopsides are very similar to the pure synthesized reference diopside (Table 2). Variations in their lattice parameters are very small and do not allow for further interpretation of possibly occurring substitution mechanisms. Compared to the reference diopside, all synthesized NH_4-bearing diopsides have a and b lattice parameters that are lower by about 1‰ relative. This is interpreted due to incorporation of small amounts of Mg replacing Ca on the M2 position. Unfortunately, our EMP and ATEM analytical data are not precise enough to confirm this assumption. There is no effect of structural defects on lattice parameters and chemical compositions, because high-resolution images of the lattice fringes display perfect crystals.

Comparison with K-bearing clinopyroxenes

There is no doubt that high pressures facilitate the incorporation of NH_4 into the diopside structure via the coupled substitution $(Ca^{2+})_{M2} + (Mg^{2+})_{M1} \Leftrightarrow (NH_4^+)_{M2} + (M^{3+})_{M1}$. The identical behavior has been observed for the analogous mechanism where K is involved instead of NH_4 (e.g., Luth, 1997; Harlow, 1997; Safonov et al., 2003; Harlow and Davies, 2004) and the extent of K incorporation indeed has been used as a geobarometer (e.g., Harlow and Veblen, 1991; Sobolev and Shatsky, 1990; Bindi et al., 2003). In comparison to NH_4, much higher amounts of K are incorporated. Experiments by Harlow (1997) at 1400 °C, 10 GPa resulted in concentrations of up to 4.7 wt% K_2O in diopside, and maximum contents at 1600 °C, 7 GPa reach about 25 mol% of Kcpx [$KM^{3+}Si_2O_6$] component (Chudinovskikh et al., 2001). The highest contents reported from a natural ultrahigh-pressure sample amount to about 17 mol% Kcpx component (Bindi et al., 2003; Harlow and Davies, 2004). Our experiments have been performed at significantly lower temperatures than that for K incorporation. However, there is overall agreement that substitution of Ca + Mg by K + M^{3+} is mainly driven by pressure and not so much by temperature (Perchuk et al., 2002; Harlow and Davies, 2004, and references therein). If so, one could speculate that higher temperatures would not induce dramatically increased NH_4 concentrations in clinopyroxenes. That NH_4 at high pressures is only incorporated as a trace component, and K as a minor or major component, might simply reflect the fact that in eight-fold coordination the ionic radius of NH_4^+ is 1.68 Å (Watenphul et al., 2009), whereas that of K^+ is 1.51 Å (Shannon, 1976). It would appear that the increase of about 10% in the ionic radius would prevent an easy incorporation of NH_4^+ into the M2 position of clinopyroxene.

There are other similarities between synthetic K- and NH_4-bearing clinopyroxenes. Cation-deficiencies in M1, i.e., Ca-Eskolaite component [$Ca_{0.5}\square_{0.5}M^{3+}Si_2O_6$], have been reported by Safonov et al. (2003; 2005), small amounts of Al-incorporation into the tetrahedron via the Ca-Tschermak's substitution $[(Mg^{2+})_{M1} + (Si^{4+})_T \Leftrightarrow (Al^{3+})_{M1} + (Al^{3+})_T]$ by Harlow (1997), Konzett and Ulmer (1999), Safonov et al. (2003, 2005), and small amounts of clinoenstatite component [$Mg_2Si_2O_6$] by Safonov et al. (2005). Harlow (1997) showed that tetrahedral substitution of Si by Cr did not occur in his experiments. Therefore, we

did not consider Cr-incorporation into the tetrahedral site as a charge balance mechanism for our NH_4-bearing diopsides.

Implications for nitrogen and hydrogen storage in the Earth's mantle

The Earth's mantle is continuously discharging nitrogen for a long time (Javoy et al., 1986; Marty, 1995; Sano et al., 2001). Degassing occurs mainly as molecular N_2. Currently, the estimated nitrogen supply from the Earth's interior to the atmosphere is estimated at about $3 \cdot 10^{10}$ mol/a (Hilton et al., 2002). This represents a very small amount compared to the atmospheric and biospheric nitrogen contents, which are higher by several orders of magnitude. While N_2 degassing is a fact, there is no sound notion about the nature of nitrogen reservoirs in mantle phases. A huge amount of investigations reports that diamonds can incorporate nitrogen by up to several thousands of ppm (e.g., De Corte et al., 1998; Davies et al., 2004), and nitrogen isotope ratios measured in diamonds, mantle xenoliths, basalts, and volcanic gases have been used to speculate about possible input of isotopically different nitrogen into the mantle via subducted sediments (e.g., Mohapatra and Murty, 2000; Pinti et al., 2001; Busigny et al., 2003a; Cartigny and Ader, 2003; Marty and Dauphas, 2003a,b; Mather et al., 2004; Thomassot et al., 2007). Busigny et al. (2003a) have shown that in blueschist and eclogite facies rocks from the Western Alps the entire nitrogen content inherited from organic material remained in the rocks, mainly as NH_4 in high-pressure phengites. Estimating the global nitrogen input they calculated that currently about 3 to $5 \cdot 10^{10}$ mol nitrogen per year are transported into the mantle via cold slab subduction. At pressures exceeding the upper stability of phengitic micas at 8 to 9 GPa and cold slab temperatures, NH_4 can be incorporated into successor K-bearing phases such as K-Si-wadeite and K-hollandite (Watenphul et al., 2009), which may be stable down to conditions of the transition zone and probably beyond. Our experiments indicate that clinopyroxene may also act as NH_4-bearing carrier downwards. The contribution of presumably K-Al-rich omphacitic clinopyroxene, typical of ultrahigh-pressure eclogites, for the nitrogen flux is probably minor because our experiments suggest that uptake of NH_4 into Al-bearing clinopyroxenes is in the order of 100 ppm at the relevant P–T-conditions. One can reasonably assume that ammonium would preferentially partition into K-richer phases such as K-bearing phengite, K-hollandite or K-Si-wadeite provided that the pressure conditions and the bulk compositions of the slab rocks allowed for the formation of these phases.

The estimations of nitrogen flux output, mainly as N_2 through mid ocean ridge basalts and volcanic arcs, and input as NH_4 via cold slabs, roughly balance each other (Hilton et al., 2002; Busigny et al., 2003a). Because a significant amount of nitrogen release occurs at mid-ocean ridges (Sano et al., 2001) a nitrogen reservoir in normal mantle rocks, i.e., peridotites, must be considered. Our experiments have shown that Cr-diopsides have an NH_4 storage capacity in the range of 500 to 1000 ppm, making them ideal candidates for nitrogen storage at depth. Clinopyroxene is stable throughout the most part of the upper mantle (e.g., Gasparik, 2003). A very rough estimation, using values for upper mantle thickness of 400 km, mean rock density of 3.5 g/cm^3, average cpx amount of 13 vol% (Koga et al., 2003), and mean concentration of 0.01 NH_4 pfu in cpx corresponding to about 500 ppm NH_4, results in the calculated nitrogen storage capacity of 10^{12} mol nitrogen for the whole upper mantle. This amount exceeds the annually recycled nitrogen by one and a

half order of magnitude but is still vanishingly small compared to the 10^{20} moles nitrogen present in the Earth's atmosphere and biosphere.

Input of ammonium by slab minerals and output as molecular nitrogen requires oxidation reactions to occur during the recycling process. The fate of any possible NH_4-silicate component at depths is subject to the redox conditions, of which no sound information is currently available. Oxidation reactions of the type

$$NH_4-\text{bearing phase} + O_2 \rightarrow \text{phase(s)} + 0.5\,N_2 + 2\,H_2O \quad (2)$$

would produce the required N_2 for degassing. Andersen et al. (1995) have shown that this actually occurs. Olivine porphyroclasts in spinel dunites from a chrome-diopside xenolith suite (Lanzarote, Canary Islands) trapped within the upper mantle have fluid inclusions containing major amounts of N_2, and some of them are pure N_2 inclusions. They interpreted that the molecular nitrogen originates from the oxidation of ammonium-bearing silicates due to increasing oxygen fugacity and/or increasing temperature, and assumed that the breakdown of phlogopite or amphibole was responsible for N_2 production. However, there is no indication of OH-bearing phases in these xenoliths, and it is quite possible that breakdown of an NH_4-bearing Cr-diopside component and oxidation to N_2 was responsible for that. Recently, Yokochi et al. (2009) reported nitrogen concentrations of mantle peridotite xenoliths from various locations worldwide. Contents amount up to 26 ppm N in phlogopite, about 0.8 ppm N in amphibole, and 0.3 ppm N in clinopyroxene, much lower than that of our synthetic diopsides from the high-pressure experiments. It is, however, important to note that these xenoliths stem from the uppermost part of the mantle, where redox conditions favor oxidation of the ammonium molecule by reaction to molecular nitrogen plus water.

NH_4 incorporation into clinopyroxene may have important implications for the water budget of the upper mantle. Water is mainly stored as OH defects in nominally anhydrous minerals. The storage capacity in upper mantle assemblages is dependent on pressure, temperature and redox conditions, and amounts from several hundred up to 4000 ppm of H_2O (e.g., Hirschmann et al., 2005; Keppler and Bolfan-Casanova, 2006; Mierdel et al., 2007). It has been experimentally shown that Cr-diopside may incorporate about 450 ppm of H_2O at upper mantle conditions (Bromiley et al., 2004), and clinopyroxenes from ultrahigh-pressure rocks may have up to 1000 ppm of H_2O (Skogby, 2006). The NH_4 component in clinopyroxene may thus significantly contribute to the upper mantle's water budget considering that, through the oxidation reaction eq. (2), one ammonium produces 0.5 N_2 + 2 H_2O, and at reducing conditions 1 NH_3 and 0.5 H_2O. Incorporation of OH^- and NH_4^+ into clinopyroxene – and potentially other mantle phases – depends, among other parameters, on the partial pressures of H_2O and NH_3. If the oxygen fugacity, f_{O_2}, is buffered by FMQ, any H–N–O fluid at relevant upper mantle conditions will consist of H_2O and N_2 (Churakov and Gottschalk, 2003a,b; and unpublished calculations; see also Simakov 1998). Fluid species rapidly change to NH_3 + H_2O at f_{O_2} of about 3 log units below FMQ. Along a normal upper mantle geotherm, increasing pressure would favor formation of NH_3. Frost and McCammon (2008) have shown that oxygen fugacities prevailing in the upper part of the upper mantle, i.e., in spinel lherzolites, are between ΔFMQ -2 and +2 log units, whereas they gradually decrease with depth attaining values of -3 to -4 log units at 4 to 6 GPa below the cratonic lithosphere, and may attain -5 log units at 8 GPa. It would thus appear that in the lower part of the upper mantle NH_3/NH_4^+ predominates in H–N–O fluids, and therefore may sta-

bilize the NH_4-component in clinopyroxene relative to N_2 plus water. Still, the contribution to the mantle's water content may be significant. If one follows this speculation, it would imply that ammonium is stored within the lower part of the upper mantle, and that some transition region would exist where pressure decrease and f_{O_2} increase would allow for gradual oxidation of the NH_4-bearing component by reaction (2). If so, this process is expected to occur somewhere in the mid-upper mantle. Qualitatively, it provides a reasonable explanation for the fact that nitrogen input – and storage – into the mantle occurs via subducted ammonium, and degassing via molecular nitrogen.

Conclusions

Our experiments show that at high pressure and reducing conditions allowing for stabilization of NH_3/NH_4^+ in H–N–O fluids ammonium, NH_4, is incorporated into diopside by the coupled substitution $(Ca^{2+})_{M2} + (Mg^{2+})_{M1} \Leftrightarrow (NH_4+)_{M2} + (M^{3+})_{M1}$. For Cr-diopside, the amount of nitrogen incorporation attains concentrations of NH_4 by up to 1000 ppm at 11.5 GPa, 750 °C. This makes clinopyroxene potentially an important carrier of ammonium in upper mantle rocks, i.e., in clinopyroxene-bearing peridotites.

Nitrogen is transported into the mantle via cold slabs through ammonium inherited from sedimentary material that is stored in K-bearing minerals, mainly micas. NH_4 remains in subducted rocks by continuous redistribution into newly formed high-pressure K-bearing phases such as phengite, K-Si-wadeite, K-hollandite, and K-Al-rich clinopyroxenes. At the other end of the deep nitrogen cycle, the mantle releases molecular nitrogen, N_2, through degassing. This occurs most probably due to oxidation of the NH_4 component in clinopyroxene at mid-upper mantle conditions. Thus, the stability of ammonium as a component in subducted slabs and mantle phases is very important for long-time, large-scale recycling of nitrogen and hydrogen between the Earth's crust and the deeper mantle.

Acknowledgements

We thank HP. Nabein and R. Schulz for technical assistance, A. Schreiber for preparation of the FIB-foils, G. Berger for preparation of the EMP samples, O. Appelt for help with the EMP work and H. Kemnitz for assistance at the SEM. Constructive reviews by V. Busigny and an anonymous reviewer helped to improve the manuscript and are highly appreciated. We thank B. Bourdon for the effective editorial handling of the manuscript. This work was supported by the German Science Foundation [He 2015/(8-1)] within the framework of the Priority Program 1236 "Structures and properties of crystals at extreme pressures and temperatures", which is gratefully acknowledged.

References

Andersen, T., Burke, E.A.J., Neumann, E.-R., 1995. Nitrogen-rich fluid in the upper mantle: fluid inclusions in spinel dunite from Lanzarote, Canary Islands. Contributions to Mineralogy and Petrology 120 (1), 20-28.

Bebout, G.E., Fogel, M.L., 1992. Nitrogen-isotope compositions of metasedimentary rocks in the Catalina schists, California: Implications for metamorphic devolatilization history. Geochimica et Cosmochimica Acta 56 (7), 2839-2849.

Bebout, G.E., Cooper, D.C., Bradley, A.D., Sadofsky, S.J., 1999. Nitrogen-isotope record of fluid-rock interactions in the Skiddaw aureole and granite, English Lake District. American Mineralogist 84, 1495-1505.

Beran, A., Libowitzky, E., 2006. Water in mantle minerals II: Olivine, garnet and accessory minerals. In: Keppler, H., and Smyth, J.R. (Eds.), Water in nominally anhydrous minerals. Reviews in Mineralogy and Geochemistry, vol. 62. Mineralogical Society of America and Geochemical Society, Chantilly, Virginia, pp. 169-191.

Bindi, L., Safonov, O.G., Litvin, Y.A., Perchuk, L.L., Menchetti, S., 2002. Ultrahigh potassium content in the clinopyroxene structure: an X-ray single crystal study. European Journal of Mineralogy 14 (5), 929-934.

Bindi, L., Safonov, O.G., Yapaskurt, V.O., Perchuk, L.L., Menchetti, S., 2003. Ultrapotassic clinopyroxene from the Kumdy-Kol microdiamond mine, Kokchetav Complex, Kazakhstan: Occurrence, composition and crystal-chemical characterization. American Mineralogist 88, 464-468.

Bromiley, G.D., Keppler, H., McCammon, C., Bromiley, F.A., Jacobsen, S.D., 2004. Hydrogen solubility and speciation in natural, gem-quality chromian diopside. American Mineralogist 89, 941-949.

Busigny, V., Cartigny, P., Philippot, P., Ader, M., Javoy, M., 2003a. Massive recycling of nitrogen and other fluid-mobile elements (K, Rb, Cs, H) in a cold slab environment: evidence from HP to UHP oceanic metasediments of the Schistes Lustrés nappe (western Alps, Europe). Earth and Planetary Science Letters 215 (1-2), 27-42.

Busigny, V., Cartigny, P., Philippot, P., Javoy, M., 2003b. Ammonium quantification in muscovite by infrared spectroscopy. Chemical Geology 198 (1-2), 21-31.

Busigny, V., Cartigny, P., Philippot, P., Javoy, M., 2004. Quantitative analysis of ammonium in biotite using infrared spectroscopy. American Mineralogist 89, 162-1630.

Cartigny, P., Ader, M., 2003. A comment on "The nitrogen record of crust-mantle interaction and mantle convection from Archean to Present" by B. Marty and N. Dauphas. Earth and Planetary Science Letters 206 (3-4), 397-410.

Chudinovskikh, L.T., Zharikov, V.A., Ishbulatov, R.A., Matveev, Y. A., 2001. Mechanism of ultrahigh potassium content incorporation into high-pressure clinopyroxene. Doklady Earth Sciences 381 (8), 956-959.

Churakov, S.V., Gottschalk, M., 2003a. Perturbation theory based equation of state for polar molecular fluids: I. Pure fluids. Geochimica et Cosmochimica Acta 67 (13), 2397-2414.

Churakov, S.V., Gottschalk, M., 2003b. Perturbation theory based equation of state for polar molecular fluids: II. Fluid mixtures. Geochimica et Cosmochimica Acta 67 (13), 2415-2425.

Davies, R.M., Griffin, W.L., O'Reilly, S.Y., McCandless, T.E., 2004. Inclusions in diamonds from the K14 and K10 kimberlites, Buffalo Hills, Alberta, Canada: diamond growth in a plume? Lithos 77 (1-4), 99-111.

De Corte, K., Cartigny, P., Shatsky, V.S., Sobolev, N.V., Javoy, M., 1998. Evidence of fluid inclusions in metamorphic microdiamonds from the Kokchetav massif, northern Kazakhstan. Geochimica et Cosmochimica Acta 62 (23-34), 3765-3773.

Fischer, T.P., Hilton, D.R., Zimmer, M.M., Shaw, A.M., Sharp, Z.D., Walker, J.A., 2002. Subduction and recycling of nitrogen along the Central American Margin. Science 297 (5584), 1154-1157.

Frost, D.J., McCammon, C.A., 2008. The redox state of Earth's mantle. Annual Review of Earth and Planetary Sciences 36, 389-420.

Gasparik, T., 2003. Phase diagrams for geoscientists – An atlas of the Earth's interior. Springer.

Griffiths, P.R., de Haseth, J.A., 1986. Fourier transform infrared spectroscopy. John Wiley and Sons. New York.

Harlow, G.E., 1997. K in clinopyroxene at high pressure and temperature: An experimental study. American Mineralogist 82, 259-269.

Harlow, G.E., Davies R.M., 2004. Status report on stability of K-rich phases at mantle conditions. Lithos 77, 647-653.

Harlow, G.E., Veblen, D.R., 1991. Potassium in clinopyroxene inclusions from diamonds. Science 251 (4994), 662-665.

Herzberg, G., 1966. Molecular spectra and molecular structure Vol.2: Infrared and Raman spectra of polyatomic molecules. Van Nostrand, Princton.

Hilton, D.R., Fischer, T.P., Marty, B., 2002. Noble gases and volatile recycling at subduction zones. In: Porcelli, D.P., Ballentine, C.J., and Wieler, R. (Eds.), Noble Gases – In geochemistry and cosmochemistry. Reviews in Mineralogy and Geochemistry, vol. 47. Mineralogical Society of America and Geochemical Society, Chantilly, Virginia, pp. 319-370.

Hirschmann, M.M., Aubaud, C., Withers, A., 2005. Storage capacity of H_2O in nominally anhydrous minerals in the upper mantle. Earth and Planetary Science Letters 236 (1-2), 167-181.

Javoy, M., Pineau, F., Delorme, H., 1986. Carbon and nitrogen isotopes in the mantle. Chemical Geology 57 (1-2), 41-62.

Keppler, H., Bolfan-Casanova, N., 2006. Thermodynamics of water solubility and partitioning. In: Keppler, H., and Smyth, J.R. (Eds.), Water in nominally anhydrous minerals. Reviews in Mineralogy and Geochemistry, vol. 62. Mineralogical Society of America and Geochemical Society, Chantilly, Virginia, pp. 193-230.

Koga, K., Hauri, E., Hirschmann, M., Bell, D., 2003. Hydrogen concentration analyses using SIMS and FTIR: Comparison and calibration for nominally anhydrous minerals. Geochemistry, Geophysics, Geosystems 4 (2), doi: 10.1029/2002GC000378.

Konzett, J., Ulmer, P., 1999. The stability of hydrous potassic phases in lherzolitic mantle – an experimental study to 9.5 GPa in simplified and natural bulk compositions. Journal of Petrology 40 (4), 629-652.

Larson, A.C., von Dreele, R.B., 2004. General structure analysis system (GSAS). Los Alamos National Laboratory Report LAUR, pp. 86-748.

Luth, R.W., 1997. Experimental study of the system phlogopite-diopside from 3.5 to 17 GPa. American Mineralogist 82, 1198-1209.

Maldener, J., Hösch, A., Langer, K., Rauch, F., 2003. Hydrogen in some natural garnets studied by nuclear reaction analysis and vibrational spectroscopy. Physics and Chemistry of Minerals 30, 337-344.

Marty, B., 1995. Nitrogen content of the mantle inferred from N_2-Ar correlation in oceanic basalts. Nature 377 (6547), 326-329.

Marty, B., Dauphas, N., 2003a. The nitrogen record of crust-mantle interaction and mantle convection from Archean to Present. Earth and Planetary Science Letters 206 (3-4), 397-410.

Marty, B., Dauphas, N., 2003b. Nitrogen isotopic composition of the present mantle and the Archean biosphere: Reply to comment by Pierre Cartigny and Magali Ader. Earth and Planetary Science Letters 216 (3), 433-439.

Mather, T.A., Allen, A.G., Bavison, B.M., Pyle, D.M., Oppenheimer, C., McGonigle, A.J.S., 2004. Nitric acid from volcanoes. Earth and Planetary Science Letters 218 (1-2), 17-30.

Mertz, L., 1965. Transformations in optics. Wiley, New York.

Mierdel, K., Keppler, H., Smyth, J.R., Langenhorst, F., 2007. Water solubility in aluminous orthopyroxene and the origin of Earth's asthenosphere. Science 315 (5836), 364-368.

Mingram, B., Bräuer, K., 2001. Ammonium concentration and nitrogen isotope composition in metasedimentary rocks from different tectonometamorphic units of the European Variscan Belt. Geochimica et Cosmochimica Acta 65 (2), 273-287.

Mohapatra, R.K., Murty, S.V.S., 2000. Search for the mantle nitrogen in the ultramafic xenoliths from San Carlos, Arizona. Chemical Geology 164 (3-4), 305-320.

Mookherjee, M., Redfern, S.A.T., Zhang, M., Harlov, D.E., 2002. Orientational order-disorder of $N(D,H)_4^+$ in tobelite. American Mineralogist 87, 1686-1691.

Pal'yanov, Y.N., Sokol, A.G., Borzdov, Y.M., Khokhryakov, A.F., Sobolev, N.V., 2002. Diamond formation through carbonate-silicate interaction. American Mineralogist 87, 1009-1013.

Perchuk, L.L., Safonov, O.G., Yapaskurt, V.O., Barton Jr., J.M., 2002. Crystal-melt equilibria involving potassium-bearing clinopyroxene as indicator of mantle-derived ultrahigh-potassic liquids: an analytical review. Lithos 60 (3-4), 89-111.

Pinti, D.L., Hashizume, K., Matsuda, J.I., 2001. Nitrogen and argon signatures in 3.8 to 2.8 Ga metasediments: Clues on the chemical state of the Archean ocean and deep biosphere. Geochimica and Cosmochimica Acta 65 (14), 2301-2315.

Plessen, B., Harlov, D.E., Henry, D., Guidotti, C.V. Ammonium loss and nitrogen isotopic fractionation in biotite as a function of metamorphic grade in metapelites from western Maine, USA. In revision.

Pöter, B., Gottschalk, M., Heinrich, W., 2004. Experimental determination of the K-NH_4-partitioning between muscovite, K-feldspar, and aqueous chloride solutions. Lithos 74 (1-2), 67-90.

Sadofsky, S.J., Bebout, G.E., 2000. Ammonium partitioning and nitrogen-isotope fractionation among coexisting micas during high-temperature fluid-rock interactions: Examples from the New England Appalachians. Geochimica et Cosmochimica Acta 64 (16), 2835-2849.

Safonov, O.G., Litvin, Y.A., Perchuk, L.L., Bindi, L., Menchetti, S., 2003. Phase relations of potassium-bearing clinopyroxene in the system $CaMgSi_2O_6 - KAlSi_2O_6$ at 7 GPa. Contributions to Mineralogy and Petrology 146 (1), 120-133.

Safonov, O.G., Perchuk, L.L., Litvin, Y.A., Bindi, L., 2005. Phase relations in the $CaMgSi_2O_6 - KAlSi_2O_6$ join at 6 and 3.5 GPa as a model for formation of some potassium-bearing deep-seated mineral assemblages. Contributions to Mineralogy and Petrology 149 (3), 316-337.

Sano, Y., Takahata, N., Nishio, Y., Fischer T.P., Williams S.N., 2001. Volcanic flux of nitrogen from the Earth. Chemical Geology 171 (3-4), 263-271.

Shannon, R.D., 1976. Revised effective ionic radii and systematic studies of interatomic distances in halides and chalcogenides. Acta Crystallographica A32, 751-767.

Simakov, S.K., 1998. Redox state of upper mantle peridotites under the ancient cratons and its connection with diamond genesis. Geochimica et Cosmochimica Acta 62 (10), 1811-1820.

Skogby, H., 2006. Water in natural mantle minerals I: Pyroxenes. In: Keppler, H., and Smyth, J.R. (Eds.), Water in nominally anhydrous minerals. Reviews in Mineralogy

and Geochemistry, vol. 62. Mineralogical Society of America and Geochemical Society, Chantilly, Virginia, pp. 155-167.

Sobolev, N.V., Shatsky, V.S., 1990. Diamond inclusions in garnets from metamorphic rocks: a new environment for diamond formation. Nature 343 (6260), 742-746.

Thomassot, E., Cartigny, P., Harris, J.P., Viljoen K.S., 2007. Methane-related diamond crystallization in the Earth's mantle: Stable isotope evidences from a single diamond-bearing xenolith. Earth and Planetary Science Letters 257 (3-4), 362-371.

Wang, W., Takahashi, E., 1999. Subsolidus and melting experiments of a K-rich basaltic composition to 27 GPa: Implication for the behavior of potassium in the mantle. American Mineralogist 84, 357-361.

Watenphul, A., Wunder, B., 2009. Temperature-dependence of the OH-stretching frequencies in topaz-OH. Physics and Chemistry of Minerals, doi 10.1007/s00269-009-0310-6.

Watenphul, A., Wunder, B., Heinrich, W., 2009. High-pressure ammonium-bearing silicates: Implications for nitrogen and hydrogen storage in the Earth's mantle. American Mineralogist 94, 283-292.

Williams, L.B., Wilcoxon, B.R., Ferrell, R.E., Sassen, R., 1992. Diagenesis of ammonium during hydrocarbon maturation and migration, Wilcox Group, Louisiana, USA. Applied Geochemistry 7 (2), 123-134.

Wirth, R., 2009. Focused Ion Beam (FIB) combined with SEM and TEM: Advanced analytical tools for studies of chemical composition, microstructure and crystal structure in geomaterials on a nanometre scale. Chemical Geology 261 (3-4), 217-229.

Yokochi, R., Marty, B., Chazot, G., Burnard, P., 2009. Nitrogen in peridotite xenoliths: Lithophile behavior and magmatic isotope fractionation. Geochimica et Cosmochimica Acta 73, 4843-4861.